7350 *Inorg. Chem.* **2009**, *48*, 7350–7358
DOI: 10.1021/ic9008009

Inorganic Chemistry
Article

A New Series of Ionic Liquids Based on the Difluorophosphate Anion

Kazuhiko Matsumoto* and Rika Hagiwara

Graduate School of Energy Science, Kyoto University, Yoshida, Sakyo-ku, Kyoto 606-8501, Japan

Received April 24, 2009

A new series of ionic liquids based on the difluorophosphate anion ($PO_2F_2^-$) has been synthesized by metathesis from the corresponding chloride. Incorporation of the $PO_2F_2^-$ anion with an *N*-heterocyclic cation (1-ethyl-3-methylimidazolium ($EMIm^+$), 1-butyl-3-methylimidazolium, 1-butyl-1-methylpyrrolidinium, or 1-butyl-1-methylpiperidinium ($BMPip^+$)) produces ionic liquids with low melting points, including some room-temperature ionic liquids. The vibrational frequencies of $PO_2F_2^-$ in the obtained ionic liquids were assigned with the aid of quantum mechanical calculations. The ionic conductivities of the ionic liquids are comparable to those of the corresponding tetrafluoroborate-based ionic liquids (e.g., 12 mS cm^{-1} for 1-ethyl-3-methylimidazolium difluorophosphate, [EMIm][PO_2F_2]). The stability of ionic liquids against hydrolysis is significantly improved by replacing the hexafluorophosphate anion with the difluorophosphate anion, which suppresses the subsequent liberation of hydrogen fluoride. According to the solvatochromic method, the donor ability of ionic liquids based on $PO_2F_2^-$ is stronger than those of ionic liquids based on BF_4^-, PF_6^-, and $N(SO_2CF_3)_2^-$, due to the large negative charge on the oxygen atoms in $PO_2F_2^-$. The electrochemical window of [EMIm][PO_2F_2] is around 4.2 V, and the diffusion coefficients of ferrocene in [EMIm][PO_2F_2] are 2.83×10^{-7} cm^2 s^{-1} by cyclic voltammetry and 3.03×10^{-7} cm^2 s^{-1} by chronoamperometry, both of which are comparable to those in 1-ethyl-3-methylimidazolium tetrafluoroborate ([EMIm][BF_4]). The X-ray structure of [BMPip][PO_2F_2] contains two cations and two anions in the asymmetric unit, where one of the two cations is disordered into two positions (chair configurations) even at −173 °C. The oxygen atoms in $PO_2F_2^-$ have closer contacts to the hydrogen atoms in $BMPip^+$ than the fluorine atoms, indicative of their stronger basicity.

Introduction

The use of ionic liquids is being increasingly extended into more fields to replace conventional aqueous or organic media. Ionic liquids often exhibit unique properties including nonflammability, negligible vapor pressure, and high thermal and chemical stability.[1,2] Recognition of ionic liquids as versatile media with ease of handling has spread after the development of air-stable room-temperature ionic liquids based on fluoroanions including BF_4^-, PF_6^-, $OSO_2CF_3^-$, and $N(SO_2CF_3)_2^-$.[3−6] Application of ionic liquids as recyclable reaction media for various organic reactions, enzyme reactions, phase separations, and extractions has been examined by many groups.[1] Ionic liquids are composed of ionic species; therefore, they often exhibit sufficient ionic conductivity without the addition of supporting electrolytes or solvents, and this has led to electrochemical applications such as lithium batteries, solar cells, fuel cells, double-layer capacitors, and plating.[2]

Although the design approach to ionic liquids varies depending on the purpose, use of the difluorophosphate anion ($PO_2F_2^-$) as a counteranion implies at least two interesting points: its structural features and its stability against hydrolysis. The preparation and characterization of a series of 1-ethyl-3-methylimidazolium ($EMIm^+$) fluorocomplex salts (BF_4^-, PF_6^-, AsF_6^-, SbF_6^-, NbF_6^-, TaF_6^-, and WF_7^-) have been previously reported.[7] The melting points of the hexafluorocomplex salts decrease with an increase in size of the anion, although these salts are classified into two different structural types in the solid state: A-type, including P, As, and Sb, and B-type, including Nb and Ta. Interestingly, [EMIm][BF_4] shows a low melting point of 15 °C (cf. 60 °C for

*To whom correspondence should be addressed. E-mail: k.matsumoto@ky7.ecs.kyoto-u.ac.jp.

(1) (a) Wilkes, J. S. *Green Chem.* **2002**, *4*, 73–80. (b) Seddon, K. R. *J. Chem. Technol. Biotechnol.* **1997**, *68*, 351–356. (c) Wasserscheid, P.; Keim, W. *Angew. Chem., Int. Ed.* **2000**, *39*, 3772–3789. (d) Hagiwara, R.; Ito, Y. *J. Fluorine Chem.* **2000**, *105*, 221–227. (e) Welton, T. *Chem. Rev.* **1999**, *99*, 2071–2084. (f) Xue, H.; Verma, R.; Shreeve, J. M. *J. Fluorine Chem.* **2006**, *127*, 159–176.

(2) Ohno, H. *Electrochemical Aspects of Ionic Liquids*; John Wiley and Sons, Inc.: Hoboken, NJ, 2005.

(3) Wilkes, J. S.; Zaworotko, M. *J. Chem. Soc., Chem. Commun.* **1992**, 965–967.

(4) Fuller, J.; Carlin, R. T.; De Long, H. C.; Haworth, D. *J. Chem. Soc., Chem. Commun.* **1994**, 299.

(5) Cooper, E. I.; Sullivan, E. J. M. *Proceedings of the 8th International Symposium on Molten Salts*; The Electrochemical Society: Pennington, NJ, 1992; Proceeding Vol. *92−16*, pp 386−396.

(6) Bonhôte, P.; Dias, A.-P.; Armand, M.; Papageorgiou, N.; Kalyanasundaram, K.; Grätzel, M. *Inorg. Chem.* **1996**, *35*, 1168–1178.

(7) (a) Matsumoto, K.; Hagiwara, R.; Yoshida, R.; Ito, Y.; Mazej, Z.; Benkič, P.; Žemva, B.; Tamada, O.; Yoshino, H.; Matsubara, S. *Dalton Trans.* **2004**, 144–149. (b) Matsumoto, K.; Hagiwara, R.; Mazej, Z.; Benkič, P.; Žemva, B. *Solid State Sci.* **2006**, *8*, 1250–1257.

Published on Web 07/06/2009

the corresponding hexafluorophosphate salt, [EMIm][PF_6]) despite the small size of the anion. The conductivity of ionic liquids is considered to be dominated by several factors such as ion size and ion−ion interactions. Even a bulky anion such as bis(trifluoromethylsulfonyl)amide ($N(SO_2CF_3)_2^-$) sometimes exhibits a relatively high conductivity when combined with an appropriate cation (e.g., 8.8 mS cm^{-1} for [EMIm][$N(SO_2CF_3)_2$]).[6] However, limited to the series of simple fluorocomplex anions above, ionic liquids with small anions exhibit high conductivity (e.g., 13 mS cm^{-1} for [EMIm][BF_4]).[8] The $PO_2F_2^-$ anion occupies an interesting position in terms of molecular design for ionic liquids, because its size is between the two popular anions, BF_4^- (T_d) and PF_6^- (O_h), and it adopts a lower symmetry compared to these anions (the distorted tetrahedral AX_2Y_2 valence shell electron pair repulsion (VSEPR) geometry (C_{2v})).

The other interesting point for $PO_2F_2^-$ is its high stability toward hydrolysis. Ionic liquids are often referred to as environmentally benign solvents or electrolytes, due to their high chemical stabilities and recyclable characteristics, described above, whereas some ionic liquids are not always environmentally benign under certain conditions. Hexafluorophosphate anion-based ionic liquids are known for their instability against hydrolysis.[9,10] For example, the room-temperature ionic liquid, 1-butyl-3-methylimidazolium hexafluorophosphate [BMIm][PF_6], gives a decomposition product, [BMIm][F]·H_2O, by hydrolytic degradation.[10] This is a characteristic of the PF_6^- salts, and there are a number of reports on the hydrolysis of PF_6^- salts, such as $LiPF_6$, used in the electrolytes of lithium ion batteries and [M(ligand)$_n$][PF_6]$_m$ (M = metal cation) salts.[11−13] According to these studies, the hydrolysis of PF_6^- yields POF_3 and $PO_2F_2^-$ accompanied by HF. The two possible chemical species in this process, POF_4^- and PO_2F, are not easily isolated, because these species are not stable under ambient conditions.[14] On the other hand, the $PO_2F_2^-$ anion, which appears as a hydrolysis product from PF_6^- even under the condition of excess water in some cases, is considered to be more stable against hydrolysis than PF_6^-,[11−13] which prevents deterioration of the system and evolution of HF and helps to improve the present chemical or electrochemical process.

This study reports the first syntheses of ionic liquids based on $PO_2F_2^-$, in addition to their spectroscopic, physical, chemical, electrochemical, and structural properties.

Results and Discussion

Syntheses, Computational Results, and Vibrational Spectra. Four *N*-heterocyclic ammonium cations, $EMIm^+$, $BMIm^+$, 1-butyl-1-methylpyrrolidinium ($BMPyr^+$), and 1-butyl-1-methylpiperidinium ($BMPip^+$), were combined with $PO_2F_2^-$ in this study (Figure 1). The $PO_2F_2^-$-based salts were obtained as colorless liquids or solids at room temperature by the simple metathesis of [K][PO_2F_2] and the corresponding chlorides in acetone. All of the ionic liquids were miscible with water under ambient conditions, so that purification through an activated alumina column was necessary to remove chloride impurities. Karl−Fisher measurements showed that the typical water contents of dried samples were less than 100 ppm.

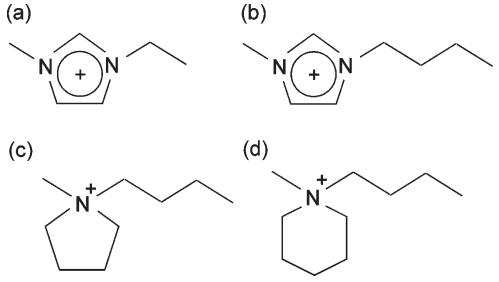

Figure 1. Chemical structures of the (a) 1-ethyl-3-methylimidazolium ($EMIm^+$), (b) 1-butyl-3-methylimidazolium ($BMIm^+$), (c) 1-butyl-1-methylpyrrolidinium ($BMPyr^+$), and (d) 1-butyl-1-methylpiperidinium ($BMPip^+$) cations.

Although the structure of $PO_2F_2^-$ was determined in several crystal structures (Table S1, Supporting Information),[13,15] including [BMPip][PO_2F_2] described below, quantum mechanical calculations were performed to obtain the basic structural parameters in the gas phase, together with those of BF_4^- and PF_6^- for comparison. All calculations performed in the current study (HF, B3LYP, PBE1PBE, MPW1PW91, and MP2) were combined with cc-pVTZ and aug-cc-pVTZ basis sets to give the same trend of geometries. The following is a brief description of $PO_2F_2^-$ based on the optimized geometries at PBE1PBE/aug-cc-pVTZ, as shown in Figure 2, with selected geometrical parameters and natural bond orbital (NBO) charges[16] (see Tables S2 and S3 for the results at the other levels, Supporting Information). The $PO_2F_2^-$ anion has an ion size between BF_4^- and PF_6^- with a P−O bond (1.481 Å) that is longer than the B−F bond in BF_4^- (1.406 Å) and with a P−F bond (1.606 Å) that is shorter than the P−F bond in PF_6^- (1.625 Å). The O−P−O (125.5°) and F−P−F (95.0°) bond angles are increased and decreased, respectively, from the ideal tetrahedral geometry, whereas the O−P−F angle (108.0°) stays close to the ideal tetrahedral angle of 109.5°, which satisfies VSEPR theory.[17]

(8) Fuller, J.; Carlin, R. T.; Osteryoung, R. A. J. *Electrochem. Soc.* **1997**, *144*, 3881–3886.
(9) Gubicza, L.; Nemestóthy, N.; Fráter, T.; Bélafi-Bakó, J. *Green Chem.* **2003**, *5*, 236–239.
(10) Swatloski, R. P.; Holbrey, J. D.; Rogers, R. D. *Green Chem.* **2003**, *5*, 361–363.
(11) (a) Tasaki, K.; Kanda, K.; Nakamura, S.; Ue, M. *J. Electrochem. Soc.* **2003**, *150*, A1628–A1636. (b) Plakhotnyk, A. V.; Ernst, L; Schmutzler, R. *J. Fluorine Chem.* **2005**, *126*, 27–31.
(12) Pérez-Salado Kamps, A. Ä.; Tuma, D.; Xia, J.; Maurer, G. *J. Chem. Eng. Data* **2003**, *48*, 746–749.
(13) Fernández-Galán, R.; Manzano, B. R.; Otero, A. *J. Organomet. Chem.* **1999**, *577*, 271–282.
(14) Christe, K. O.; Dixon, D. A.; Schrobilgen, G. J.; Wilson, W. W. *J. Am. Chem. Soc.* **1997**, *119*, 3918–3928.
(15) (a) Harrison, R. W.; Thompson, R. C.; Trotter, J. *J. Chem. Soc. A* **1966**, 1775–1780. (b) Trotter, J.; Whitlow, S. H. *J. Chem. Soc. A* **1967**, 1383–1386. (c) Harrison, R. W.; Trotter, J. *J. Chem. Soc. A* **1969**, 1783–1787. (d) Fessler, Th, U.; Hiibener, R.; J.; Strahle, Z. *Anorg. Allg. Chem.* **1997**, *623*, 1367–1374. (e) Chen, L.; Khan, M. A.; Richter-Addo, G. B. *Inorg. Chem.* **1998**, *37*, 533–540. (f) Gregson, C. K. A.; Long, N. J.; White, A. J. P.; Williams, D. J. *Organometallics* **2004**, *23*, 3674–3682. (g) Fernández-Galán, R.; Manzano, B. R.; Otero, A.; Lanfranchi, M.; Pellinghelli, M. A. *Inorg. Chem.* **1994**, *33*, 2309–2312.
(16) (a) Reed, A. E.; Weinstock, R. B.; Weinhold, F. *J. Chem. Phys.* **1985**, *83*, 735–746. (b) Reed, A. E.; Curtiss, L. A.; Weinhold, F. *Chem. Rev.* **1998**, *88*, 899–926. (c) Glendening, E. D.; Reed, A. E.; Carpenter, J. E.; Weinhold, F. *NBO*, version 3.1; Gaussian, Inc.: Pittsburgh, PA, 1990. (d) Glendening, E. D.; Badenhoop, J. K.; Reed, A. E.; Carpenter, J. E.; Bohmann, C. M.; Morales, C. M.; Weinhold, F. *NBO*, version 5.0; Theoretical Chemistry Institute, University of Wisconsin: Madison, WI, 2001.
(17) (a) Gillespie, R. J.; Popelier, P. L. A. *Chemical Bonding and Molecular Geometry*; Oxford University Press, New York, 2001; p 191. (b) Gillespie, R. J.; Hargittai, I. *The VSEPR Model of Molecular Geometry*; Allyn and Bacon: Boston, MA, 1991.

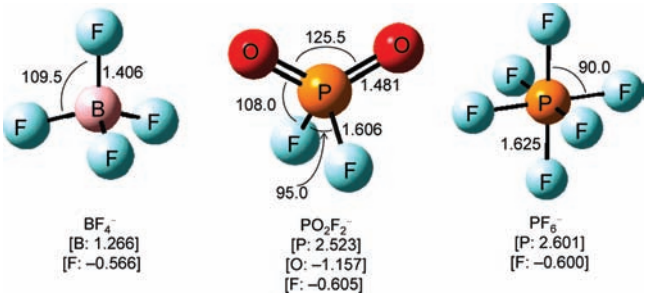

Figure 2. Calculated geometries of (a) BF_4^-, (b) $PO_2F_2^-$, and (c) PF_6^- at PBE1PBE/aug-cc-pVTZ (Å, deg). Numbers in the brackets represent the NBO charges.

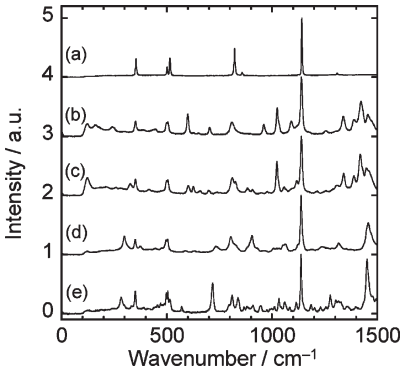

Figure 3. Raman spectra of (a) $[K][PO_2F_2]$, (b) $[EMIm][PO_2F_2]$, (c) $[BMIm][PO_2F_2]$, (d) $[BMPyr][PO_2F_2]$, and (e) $[BMPip][PO_2F_2]$ at room temperature.

According to the NBO analysis, the charges on the fluorine atoms in $PO_2F_2^-$ are close to those in PF_6^- and slightly more negative than those in BF_4^-. The oxygen atoms in $PO_2F_2^-$ are almost twice as negatively charged compared with the fluorine atoms in the three anions.

Raman and infrared (IR) spectra of the $PO_2F_2^-$ salts recorded at room temperature, where $[EMIm][PO_2F_2]$ and $[BMIm][PO_2F_2]$ are liquid and $[BMPyr][PO_2F_2]$ and $[BMPip][PO_2F_2]$ are solid, are shown in Figures 3 and 4, respectively. To our knowledge, this is the first detailed assignment for the vibrational frequencies of $PO_2F_2^-$ based on quantum mechanical calculations (Table 1 and Table S4, Supporting Information).[13,18,19] The vibrational modes of the $PO_2F_2^-$ anion belong to the irreducible representations $\Gamma = 4A_1 + A_2 + 2B_1 + 2B_2$ under C_{2v} symmetry. For the Raman spectra of the $PO_2F_2^-$ salts, the assignments of the four modes, $\nu_{as}(PO_2)$, $\nu_s(PO_2)$, $\nu_{as}(PF_2)$, and $\nu_s(PF_2)$ + small $\nu_s(PO_2)$, are straightforward, whereas the three modes, $\delta_s(PF_2) - \delta_s(PO_2)$, $\rho_r(PF_2) - \rho_w(PO_2)$, and $\rho_w(PF_2) - \rho_r(PO_2)$, are indistinguishable and assigned to the two observed bands around 500 cm^{-1}. The $\delta_s(PF_2) + \delta_s(PO_2)$ and $\rho_t(PF_2) - \rho_t(PO_2)$ modes are also assigned to the one observed band around 350 cm^{-1}. The IR spectra of the $PO_2F_2^-$ salts are characterized by four strong absorption bands. The two modes, $\nu_{as}(PF_2)$ and $\nu_s(PF_2)$ + small $\delta_s(PO_2)$, overlap with each other around 820 cm^{-1}. The vibrational modes around 500 cm^{-1} ($\delta_s(PF_2) - \delta_s(PO_2)$, $\rho_r(PF_2) - \rho_w(PO_2)$, and $\rho_w(PF_2) - \rho_r(PO_2)$) are also observed as one broad band. Compared to the isoelectronic SO_2F_2 molecule (S−O = 1.386 Å, S−F = 1.514 Å, O−S−O = 124.63°, O−S−F = 107.67°, F−S−F = 98.62°, and O−S−F = 107.60 °),[20] the vibrational frequencies for $PO_2F_2^-$ are observed at lower frequencies, where the $\nu_{as}(AO_2)$ mode (A = S or P) exhibits the largest difference (200 cm^{-1}).[21,22]

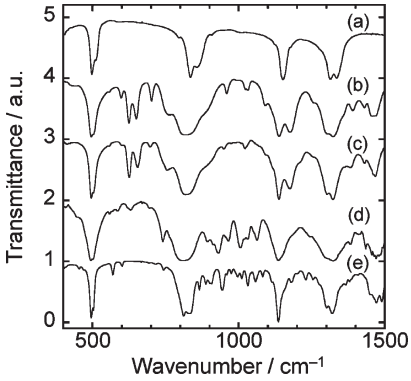

Figure 4. Infrared spectra of (a) $[K][PO_2F_2]$, (b) $[EMIm][PO_2F_2]$, (c) $[BMIm][PO_2F_2]$, (d) $[BMPyr][PO_2F_2]$, and (e) $[BMPip][PO_2F_2]$ at room temperature.

In all of the *N*-heterocyclic ammonium salts examined, the $PO_2F_2^-$ anion exhibits similar vibrational frequencies with similar relative intensities, whereas there are several shifts for some vibrational modes containing $P-O_2$ and $P-F_2$ stretching between the potassium salt and the quaternary ammonium salts. This shift arises from the weakened interaction between the cation and the oxygen or fluorine atom in the anion by introducing the bulky *N*-heterocyclic ammonium cation with delocalized positive charges.

Physical and Chemical Properties. The physical properties of the present ionic liquids are summarized in Table 2, in addition to those of $[EMIm][BF_4]$ and $[BMIm][PF_6]$ for comparison. Molar volume calculated from the measured density increases with the increase in cation size. The order of molar volume for the three room-temperature ionic liquids, $[BMIm][BF_4]$ (188 $cm^3\ mol^{-1}$)[23] < $[BMIm][PO_2F_2]$ (195 $cm^3\ mol^{-1}$) < $[BMIm][PF_6]$ (207 $cm^3\ mol^{-1}$),[23] is in agreement with the values expected from the sizes of the three anions.

The differential scanning calorimetry (DSC) results are shown in Figure 5. The melting point observed for the $EMIm^+$ salt ($[EMIm][PO_2F_2]$ (7 °C)), which is lower than that for the corresponding $BMIm^+$ salt ($[BMIm][PO_2F_2]$ (19 °C)), is contrary to that for the BF_4^-- (15 °C for $[EMIm][BF_4]$[8] and −83 °C (glass transition) for $[BMIm][BF_4]$[23,24]) and PF_6^--based (60 °C for $[EMIm][PF_6]$[6] and 10 °C for $[BMIm][PF_6]$[23]) salts, whereas the $OSO_2CF_3^-$- and $N(SO_2CF_3)_2^-$-based salts show the same behavior (−9 °C for $[EMIm][OSO_2CF_3]$,[6] 17 °C for $[BMIm][OSO_2CF_3]$,[23] −18 °C for $[EMIm][N(SO_2CF_3)_2]$,[23] and −3 °C for $[BMIm][N(SO_2CF_3)_2]$[25]). The

(18) Bühler, V. K.; Bues, W. *Z. Anorg. Allg. Chem.* **1961**, *308*, 62–71.
(19) Addou, A.; Vast, P.; Legrand, P. *Spectrochim. Acta* **1982**, *38A*, 785–790.
(20) Mootz, D.; Merschenzquack, A. *Acta Crystallogr.* **1988**, *C44*, 924–925.
(21) Birchall, T.; Gillespie, R. J. *Spectrochim. Acta* **1966**, *22*, 681–688.
(22) Lide, D. R. Jr.; Mann, D. E.; Comeford, J. J. *Spectrochim. Acta* **1965**, *21*, 497–501.
(23) Tokuda, H.; Hayamizu, K.; Ishii, K.; Susan, M. A. B. H.; Watanabe, M. *J. Phys. Chem. B* **2004**, *108*, 16593–16600.
(24) Holbrey, J. D.; Seddon, K. R. *J. Chem. Soc., Dalton Trans.* **1999**, 2133–2139.
(25) Tokuda, H.; Hayamizu, K.; Ishii, K.; Susan, M. A. B. H.; Watanabe, M. *J. Phys. Chem. B* **2005**, *109*, 6103–6110.

Table 1. Vibrational Frequencies, Intensities, and Assignments for the $PO_2F_2^-$ Anion at 25 °C[a]

K^{+b}		$EMIm^{+c}$		$BMIm^{+c}$		$BMPyr^{+d}$		$BMPip^{+c}$			
Raman	IR	Raman	IR	Raman	IR	Raman	IR	Raman	IR	calcd[e]	assignment[f] (C_{2v})
1308.9(4)	1335(s) 1312(s)	n.d.	1323(s)	n.d.	1325(s)	n.d.	1316(s)	n.d.	1320(s) 1300(s)	1328.0(3)[366]	$\nu_{as}(PO_2)$
1141.6(100)	11452(s)	1139.6(100)	1140(s)	1139.6(100)	1138(s)	1138.2(100)	1136(s)	1137.7(100)	1136(s)	1125.0(38)[180]	$\nu_s(PO_2)$
857.1(5)	857(sh)	n.d.	820(s)	n.d.	818(s)	n.d.	812(s)	n.d.	832(s)	784.9(2)[241]	$\nu_{as}(PF_2)$
821.9(48)	835(s)	807.4(20)		811.8(27)		803.6(27)		810.3(29)	812(s)	773.7(12)[134]	$\nu_s(PF_2)$ + small $\delta_s(PO_2)$
514.7(30)	500(s)	504.1(10)	498(s)	505.1(23)	498(s)	504.1(22)	494(s)	504.6(34)	504(s)	486.0(2)[32]	$\delta_s(PF_2) - \delta_s(PO_2)$
501.7(17)		498.8(sh)		499.3(sh)		495.9(sh)		497.9(30)	496(s)	479.0(1)[27]	$\rho_r(PF_2) - \rho_w(PO_2)$
										473.6(1)[29]	$\rho_w(PF_2) - \rho_r(PO_2)$
										331.5(1)[1]	$\delta_s(PF_2) + \delta_s(PO_2)$
353.7(29)		351.7(20)		351.3(21)		349.3(19)		350.3(31)		330.9(1)[0]	$\rho_t(PF_2) - \rho_t(PO_2)$

[a] Frequencies are given in cm^{-1}. The experimental intensities for the Raman spectra are scaled relative to the intensity of the $\nu_s(PO_2)$ mode of $PO_2F_2^-$, which is assigned a value of 100. The abbreviations sh, br, w, m, and s denote shoulder, broad, weak, medium, and strong. Vibrational modes assigned to the cation or combination modes and overtones are summarized in the Supporting Information. [b] Solid (crystal phase) at 25 °C. [c] Liquid at 25 °C. [d] Solid (plastic phase) at 25 °C. [e] MP2/aug-cc-pVTZ. Values in parentheses are Raman intensities ($Å^4$ amu^{-1}), and values in square brackets are infrared intensities (km mol^{-1}). [f] The symbols ν_{as}, ν_s, δ_s, ρ_r, ρ_w, and ρ_t denote asymmetric stretching, symmetric stretching, scissoring, rocking, wagging, and twisting modes, respectively.

Table 2. Physical Properties of PO_2F_2-Based Salts[a]

salt	T_m/°C	T_d/°C	ρ/g cm^{-3}	η/cP	MV /cm^3 mol^{-1}	σ/mS cm^{-1}	Λ/S cm^2 mol^{-1}
[EMIm][PO_2F_2]	7	323	1.314	35	161	12	1.9
[BMIm][PO_2F_2]	19	320	1.230	75	195	3.2	0.62
[BMPyr][PO_2F_2]	27	313	1.165	102	209	3.6	0.76
[BMPip][PO_2F_2]	41	297	1.156	410	223	0.90	0.20
[EMIm][BF_4][b]	15	360	1.280	34	156	13	2.0
[BMIm][PF_6][c]	10 (T_g: −77)	433	1.371	261	207	1.5	0.31

[a] T_m, melting point; T_g, glass transition temperature; and T_d, thermal decomposition temperature (5% weight loss). The density (ρ), viscosity (η), molar volume (MV), conductivity (σ), and molar conductivity (Λ) values are at 25 °C for [EMIm][PO_2F_2] and [BMIm][PO_2F_2], at 35 °C for [BMPyr][PO_2F_2], and at 45 °C for [BMPip][PO_2F_2]. [b] Refs 7 and 8. [c] Ref 23.

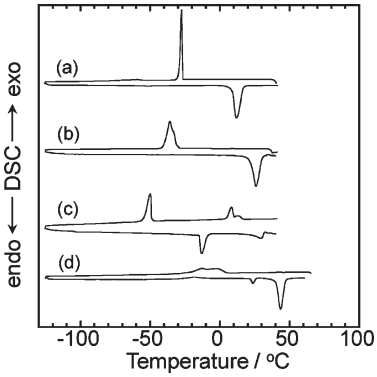

Figure 5. Differential scanning calorimetric thermograms for (a) [EMIm][PO_2F_2], (b) [BMIm][PO_2F_2], (c) [BMPyr][PO_2F_2], and (d) [BMPip][PO_2F_2].

low melting points of 27 and 41 °C for the nonaromatic cation-based salts, [BMPyr][PO_2F_2] and [BMPip][PO_2F_2], are noteworthy when compared to those for [BMPyr][BF_4] (138 °C),[26] [BMPyr][PF_6] (70 °C),[27] and [BMPip][BF_4] (146 °C).[28] Both [BMPyr][PO_2F_2] and [BMPip][PO_2F_2] undergo a solid−solid phase transition before melting, as is often observed for such nonaromatic cations.[26,27,29−31] In the DSC curve of [BMPyr][PO_2F_2], a peak ascribed to a crystal−plastic crystal phase transition is observed at −15 °C. Alkylpyrrolidinium cations have a high symmetry around the nitrogen atom and often form plastic crystal phases.[26,27,29] Timmermans pointed out that the entropy change of fusion, ΔS_{fus}, is usually less than 20 J K^{-1} mol^{-1} for plastic crystal phases.[32] For [BMPyr][PO_2F_2], a ΔS_{fus} of 12.8 J K^{-1} mol^{-1} calculated according to the relationship $\Delta S_{fus} = \Delta H_{fus}/T_m$, where the enthalpy change of fusion, $\Delta_{fus}H$, and T_m are 3849 J mol^{-1} and 300 K, respectively, satisfies this condition. The X-ray diffraction patterns measured at −120 and −30 °C show that [BMPyr][PO_2F_2] has the same crystalline phase at these temperatures, whereas the diffraction pattern at 0 °C contains only several peaks in the small 2θ region, which suggests a plastic crystalline structure for this phase (Figure S1 and Table S5, Supporting Information). Although alkylpiperidinium-based salts sometimes also form a plastic phase, the X-ray diffraction pattern of [BMPip][PO_2F_2] revealed that both of the solid phases observed in the DSC thermograms are crystalline; that is, the endothermic peak at 22 °C during the heating process is ascribed to a crystal−crystal phase transition (see the section labeled Crystal Structure of [BMPip][PO_2F_2]). The melting point of a pure salt is

(26) Forsyth, S.; Golding, J.; MacFarlane, D. R.; Forsyth, M. *Electrochim. Acta* **2001**, *46*, 1753–1757.
(27) Golding, J.; Hamid, N.; MacFarlane, D. R.; Forsyth, M.; Forsyth, C.; Collins, C.; Huang, J. *Chem. Mater.* **2001**, *13*, 558–564.
(28) Zhou, Z. B.; Matsumoto, H.; Tatsumi, K. *Chem.—Eur. J.* **2006**, *12*, 2196–2212.
(29) MacFarlane, D. R.; Meakin, P.; Sun, J.; Amini, N.; Forsyth, M. *J. Phys. Chem. B* **1999**, *103*, 4164–4170.
(30) Henderson, W. A.; Young, V. G. Jr.; Fylstra, P.; De Long, H. C.; Trulove, P. C. *Cryst. Growth Des.* **2006**, *6*, 1645–1648.
(31) Henderson, W. A.; Young, V. G. Jr.; Passerini, S.; Trulove, P. C.; De Long, H. C. *Chem. Mater.* **2006**, *18*, 934–938.
(32) Timmermans, J. *J. Phys. Chem. Solids* **1961**, *181*, 1–8.

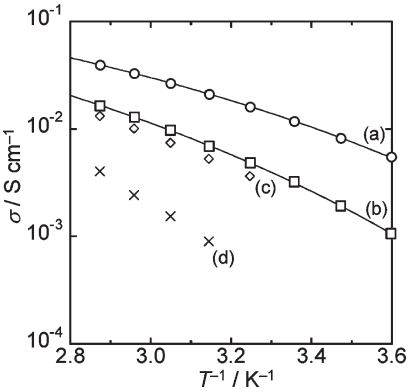

Figure 6. Arrhenius plots of ionic conductivity for (a) [EMIm][PO_2F_2], (b) [BMIm][PO_2F_2], (c) [BMPyr][PO_2F_2], and (d) [BMPip][PO_2F_2]. The solid lines are fitting curves based on the VTF equation.

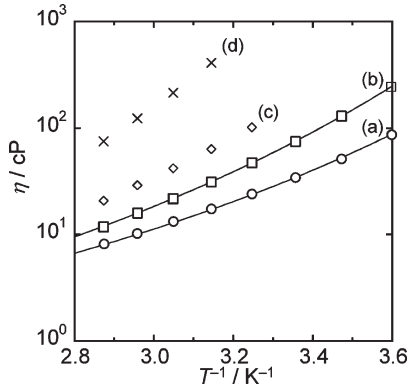

Figure 7. Arrhenius plots of viscosity for (a) [EMIm][PO_2F_2], (b) [BMIm][PO_2F_2], (c) [BMPyr][PO_2F_2], and (d) [BMPip][PO_2F_2]. The solid lines are fitting curves based on the VTF equation.

dominated by the balance of its lattice and solvation energies.[33] The relatively low melting points for the present $PO_2F_2^-$ salts suggest larger solvation energies compared to the lattice energies. The thermal decomposition temperatures of the four ionic liquids were determined by thermogravimetric analysis at the temperature where the sample loses 5% of its weight (Figure S2, Supporting Information). Two imidazolium-based salts, [EMIm][PO_2F_2] and [BMIm][PO_2F_2], exhibited a similar decomposition temperature around 320 °C. The other two ionic liquids, [BMPyr][PO_2F_2] and [BMPip][PO_2F_2], were slightly less stable than the imidazolium-based salts.

Arrhenius plots of ionic conductivity for [EMIm][PO_2F_2], [BMIm][PO_2F_2], [BMPyr][PO_2F_2], and [BMPip][PO_2F_2] are shown in Figure 6. The ionic conductivity of [EMIm][PO_2F_2] is 12 mS cm^{-1} at 25 °C, which is close to the 13 mS cm^{-1} for [EMIm][BF_4][7,8] and higher than those of other reported room-temperature ionic liquids based on fluoroanions (e.g., 6.2 mS cm^{-1} for [EMIm][SbF_6],[7] 8.5 mS cm^{-1} for [EMIm][NbF_6],[7] 7.1 mS cm^{-1} for [EMIm][TaF_6],[7] 8.6 mS cm^{-1} for [EMIm][OSO_2CF_3],[6] and 8.8 mS cm^{-1} for [EMIm][$N(SO_2CF_3)_2$][6]). The ionic conductivity of 3.2 mS cm^{-1} for [BMIm][PO_2F_2] at 25 °C is also comparable to the 3.6 mS cm^{-1} for [BMIm][BF_4].[23] For [EMIm][PO_2F_2] and [BMIm][PO_2F_2], the plots show slightly convex curves in the temperature range of measurement. The Vogel−Tamman−Fulcher (VTF) equation[34] (eq 1) is known to fit the behavior of ionic conductivity for ionic liquids better than the Arrhenius equation:[23,24,35,36]

$$\sigma = \sigma_0 \exp[-B/(T - T_0)] \quad (1)$$

where σ is ionic conductivity (S cm^{-1}) and σ_0 (S cm^{-1}), B (K), and T_0 (K) are constants. In the current study, only the ionic conductivities of [EMIm][PO_2F_2] and [BMIm][PO_2F_2] were fitted by the VTF equation, because the temperature range of measurement was sufficiently wide (5−75 °C). Arrhenius plots of viscosity for [EMIm][PO_2F_2], [BMIm][PO_2F_2], [BMPyr][PO_2F_2], and [BMPip][PO_2F_2] are shown in Figure 7. The plots are slightly concave curves in this case and could also be fitted by the VTF equation (eq 2) for [EMIm][PO_2F_2] and [BMIm][PO_2F_2]:

$$\eta = \eta_0 \exp[B/(T - T_0)] \quad (2)$$

where η is viscosity (cP) and η_0 (cP), B (K), and T_0 (K) are constants. Both the ionic conductivity and viscosity for [EMIm][PO_2F_2] and [BMIm][PO_2F_2] are fitted well by the VTF equations, and the best-fit parameters obtained for the present ionic liquids are shown in Table S6 (Supporting Information). As previously reported for both ionic conductivity and viscosity,[23,25,35,36] a more prominent change is observed for B compared with T_0 by changing the cation. It is known that most ionic liquids obey Walden's equation, $\Lambda\eta = a$, where a is a constant called the Walden product and Λ is the molar conductivity.[37−40] The Walden product (in [S cm^2 mol^{-1}][cP]) of 67 for [EMIm][PO_2F_2] is close to those for other known ionic liquids (e.g., 68 for [EMIm][BF_4],[8] 78 for [EMIm][SbF_6],[7] 79 for [EMIm][NbF_6],[7] 67 for [EMIm][TaF_6],[7] and 77 for [EMIm][$N(SO_2CF_3)_2$][6]), which suggests that the ion conduction in these ionic liquids is dominated by the same mechanism.

The higher stability of $PO_2F_2^-$-based ionic liquids against hydrolysis compared with PF_6^--based ionic liquids was demonstrated by adding water to [BMIm][PO_2F_2] and [BMIm][PF_6] at elevated temperatures. A glass vial containing 1 mL of [BMIm][PO_2F_2] or [BMIm][PF_6] was heated up to 130 °C, and 0.3 mL of H_2O was added to it. As previously reported,[9,10] [BMIm][PF_6] was quickly hydrolyzed under these conditions to yield white fumes of HF and a yellowish decomposed liquid with severe etching of the glass vial. On the other hand,

(33) Krossing, I.; Slattery, J. M.; Daguenet, C.; Dyson, P. J.; Oleinikova, A.; Weingärtner, H. *J. Am. Chem. Soc.* **2006**, *128*, 13427–13434.
(34) (a) Vogel, H. *Phys. Z.* **1921**, *22*, 645–646. (b) Fulcher, G. S. *J. Am. Ceram. Soc.* **1923**, *8*, 339–355.
(35) Tokuda, H.; Ishii, K.; Susan, M. A. B. H.; Tsuzuki, S.; Hayamizu, K.; Watanabe, M. *J. Phys. Chem. B* **2006**, *110*, 2833–2839.
(36) Noda, A.; Hayamizu and, K.; Watanabe, M. *J. Phys. Chem. B* **2001**, *105*, 4603–4610.
(37) (a) Walden, P.; Ulich, H.; Busch, G. *Z. Phys. Chem.* **1926**, *123*, 429–434. (b) Walden, P.; Birr, E. J. *Z. Phys. Chem. Abt. A* **1931**, *153*, 1–51.
(38) Hagiwara, R.; Matsumoto, K.; Nakamori, Y.; Tsuda, T.; Ito, Y.; Matsumoto, H.; Momota, K. *J. Electrochem. Soc.* **2003**, *150*, D195.
(39) Yoshida, Y.; Muroi, K.; Ohtsuka, A.; Saito, G.; Takahashi, M.; Yoko, T. *Inorg. Chem.* **2004**, *43*, 1458–1462.
(40) Xu, W.; Cooper, E. I.; Angell, C. A. *J. Phys. Chem. B* **2003**, *107*, 6170–6178.

Table 3. Absorption Maximum Wavelength (λ_{Cu}) of [Cu(tmen)(acac)][BPh_4] in Selected Ionic Liquids

ionic liquid	λ_{Cu}/nm[a]
[EMIm][PO_2F_2]	625
[EMIm][BF_4]	537
[EMIm][$N(SO_2CF_3)_2$]	545
[BMIm][PO_2F_2]	627
[BMIm][BF_4]	541
[BMIm][PF_6]	516
[BMIm][$N(SO_2CF_3)_2$]	547

[a] The concentration of [Cu(tmen)(acac)][BPh_4] is 0.01 mol L^{-1}.

[BMIm][PO_2F_2] did not display any change in appearance under the same conditions, except for the evaporation of H_2O (Figure S3, Supporting Information). According to the results of ^{31}P NMR spectroscopy, [BMIm][PF_6], which was kept in a PFA (tetrafluoroethylene-perfluoroalkylvinylether copolymer) container at 150 °C for 1 h with occasional addition of H_2O, was completely hydrolyzed (Figure S4, Supporting Information). On the other hand, the ^{31}P NMR spectrum of the [BMIm][PO_2F_2] sample after the same treatment was identical to that of the original sample (Figure S4, Supporting Information).

Donor Property. The polarity of ionic liquids has been measured using several methods, such as in the cases of organic solvents.[6,41−47] Although the definition of polarity for ionic liquids is quite complicated due to the presence of two components, cation and anion, solvatochromic methods provide a simple and easy scale to evaluate the donor or acceptor properties of ionic liquids. The square-planar complex salt, [Cu(tmen)(acac)][BPh_4] (tmen = *N*,*N*,*N*′,*N*′-tetramethylethylenediamine, acac = acetylacetonate, and BPh_4 = tetraphenylborate), shows an absorption peak for the lowest energy d−d band in the visible range, and the position of the maximum wavelength (λ_{Cu}) depends on the donor property of the solvent or the ionic species in a solvent.[48] Table 3 shows λ_{Cu} for selected ionic liquids based on $EMIm^+$ and $BMIm^+$. Figure 8 shows visible absorption spectra of [Cu(tmen)(acac)][BPh_4] in $BMIm^+$-based ionic liquids (0.01 mol L^{-1}; see Figure S5 for the spectra including $EMIm^+$-based ionic liquids, Supporting Information). The λ_{Cu} values obtained for the ionic liquids based on BF_4^-, PF_6^-, and $N(SO_2CF_3)_2^-$ are in good agreement with the reported values.[41,43,47] It is known that λ_{Cu} is insensitive to the cationic structure, because the copper center accepts an electron donor, namely, the anion in the ionic liquids. The PF_6^- anion shows low nucleophilicity due to its high symmetry (O_h) and low charge density. A low-

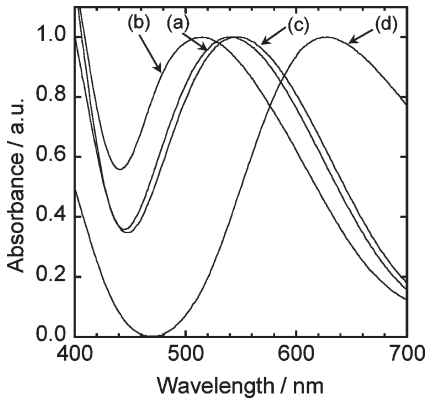

Figure 8. Visible absorption spectra of [Cu(tmen)(acac)][BPh_4] in $BMIm^+$-based ionic liquids: (a) [BMIm][BF_4], (b) [BMIm][PF_6], (c) [BMIm][$N(SO_2CF_3)_2$], and (d) [BMIm][PO_2F_2]. Concentration: 0.01 mol L^{-1}.

ering in symmetry for BF_4^- slightly increases its donor property. Although the bulky $N(SO_2CF_3)_2^-$ anion has delocalized charge density, the negatively charged parts such as O and N atoms can function as electron donors, resulting in its similar donor property to that of BF_4^-. The ionic liquids based on $PO_2F_2^-$ exhibit significantly large λ_{Cu} values (625 nm for [EMIm][PO_2F_2] and 627 nm for [BMIm][PO_2F_2]) that are close to the 638 nm observed for the strong donor, $CF_3CO_2^-$, in [BMIm][CF_3CO_2][41] and close to the 623 nm observed for pyridine, which is known as a Lewis basic solvent.[48] The results of quantum mechanical calculations (Figure 1) indicate that the oxygen atoms have a negative charge twice as large as that of the fluorine atoms in $PO_2F_2^-$ and can strongly interact with the copper center, resulting in a large λ_{Cu} value. The correlation between λ_{Cu} and the degree of dissociation of the ions in ionic liquids was previously evaluated and reported as showing a trend where the degree of dissociation decreases with the increase in λ_{Cu} (i.e., the donor property of the anion).[41] The high ionic conductivity for ionic liquids based on $PO_2F_2^-$, despite the large λ_{Cu} value, implies potentially high diffusion coefficients of the ionic species.

Electrochemical Properties of [EMIm][PO_2F_2]. The electrochemical properties of [EMIm][PO_2F_2], which exhibited the highest conductivity in the present series, were investigated by voltammetric methods. A linear sweep voltammogram of a glassy carbon disk electrode in [EMIm][PO_2F_2] at 25 °C is shown in Figure 9 (see Figure S6 for a voltammogram using a platinum electrode, Supporting Information). The linear sweep voltammogram does not show any peaks that would be attributed to possible impurities. The cathode and anode limits of this ionic liquid are −2.6 and 1.7 V versus the Fc^+/Fc redox couple, respectively, when the limits were determined as the potential of a glassy carbon electrode, where the absolute values of the current densities exceeded 0.5 mA cm^{-2} during linear sweep voltammetry at a scan rate of 5 mV s^{-1}. Both the cathode and anode stabilities are comparable to those of $EMImBF_4$,[2,49] which implies its

(41) Tokuda, H.; Tsuzuki, S.; Susan, M. A. B. H.; Hayamizu, K.; Watanabe, M. *J. Phys. Chem. B* **2006**, *110*, 19593–19600.
(42) Aki, S. N. V. K.; Brennecke, J. F.; Samanta, A. *Chem. Commun.* **2001**, 413–414.
(43) Muldoon, M. J.; Gordon, C. M.; Dunkin, I. R. *J. Chem. Soc., Perkin Trans. 2* **2001**, 433–435.
(44) Dzyuba, S. V.; Bartsch, R. A. *Tetrahedron Lett.* **2002**, *43*, 4657–4659.
(45) Crowhurst, L.; Mawdsley, P. R.; Arlandis, J. M. P.; Salter, P. A.; Welton, T. *Phys. Chem. Chem. Phys.* **2003**, *5*, 2790–2794.
(46) Carmichael, A. J.; Seddon, K. R. *J. Phys. Org. Chem.* **2000**, *13*, 591–595.
(47) Wasserscheid, P.; Gordon, C. M.; Hilgers, C.; Muldoon, M. J.; Dunkin, I. R. *Chem. Commun.* **2001**, 1186–1187.
(48) (a) Fukuda, Y.; Sone, K. *Bull. Chem. Soc. Jpn.* **1972**, *45*, 465–469. (b) Soukup, R. W.; Sone, K. *Bull. Chem. Soc. Jpn.* **1987**, *60*, 2286–2288. (c) Linert, W.; Jameson, R. F.; Taha, A. *J. Chem. Soc., Dalton Trans.* **1993**, 3181–3186.
(49) (a) Nakagawa, H.; Izuchi, S.; Kuwana, K.; Nukuda, T.; Aihara, Y. *J. Electrochem. Soc.* **2003**, *150*, A695–A700. (b) Katayama, Y.; Dan, S.; Miura, T.; Kishi, T. *J. Electrochem. Soc.* **2001**, *148*, C102–C105.

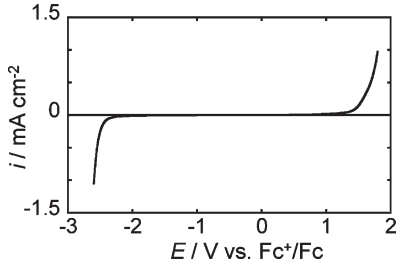

Figure 9. Linear sweep voltammogram of a glassy carbon electrode in [EMIm][PO_2F_2]. Scan rate: 5 mV s^{-1}.

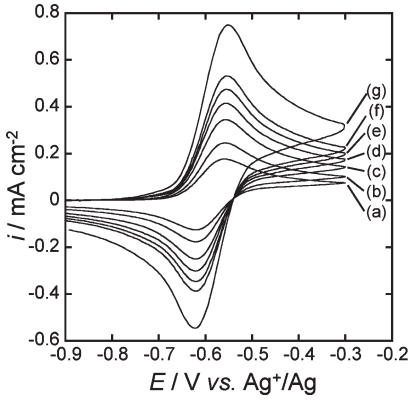

Figure 10. Cyclic voltammogram of a platinum electrode in [EMIm][PO_2F_2] containing 16.7 mmol L^{-1} of ferrocene. Scan rate: (a) 5, (b) 10, (c) 20, (d) 30, (e) 40, (f) 50, and (g) 100 mV s^{-1}.

potential applications as an electrolyte in energy conversion devices.

The redox behavior of the Fc^+/Fc couple in [EMIm][PO_2F_2] was further investigated using cyclic voltammetry and chronoamperometry with a platinum disk electrode at 25 °C to demonstrate the electrochemical behavior of chemical species in the ionic liquid. The electrochemical parameters (Table S7, Supporting Information) and shape of the cyclic voltammogram (Figure 10) indicate the high reversibility of the Fc^+/Fc redox couple in [EMIm][PO_2F_2]. The redox potential of the Fc^+/Fc couple was −0.590 V versus Ag^+/Ag under the present experimental conditions. The diffusion coefficient of ferrocene at 25 °C in [EMIm][PO_2F_2] was independently evaluated using cyclic voltammetry and chronoamperometry with eqs 3 and 4, respectively:[50]

$$i_p = (2.69 \times 10^5) n^{3/2} D^{1/2} v^{1/2} C \quad (3)$$

$$i_d = (9.65 \times 10^5) n D^{1/2} t^{-1/2} C \pi^{-1/2} \quad (4)$$

where i_p is the anodic peak current density in the cyclic voltammogram, i_d is the anodic current density at time t in the chronoamperogram, n is the number of electrons involved in the electrode reaction ($n = 1$), D is the diffusion coefficient, v is the scan rate, and C is the concentration (see Figures S7 and S8 for the $v^{1/2}$−i_p and $t^{-1/2}$−i_d plots, respectively, Supporting Information). The diffusion coefficients determined by cyclic voltammetry (2.8×10^{-7} cm^2 s^{-1}) and chronoamperometry (3.0×10^{-7} cm^2 s^{-1}) agree well with each other and are comparable to some of the data determined for [EMIm][BF_4] (2.9×10^{-7} and 3.2×10^{-7}),[51,52] which reflect viscosities that are almost the same (Table 2) as those of the two ionic liquids and a similar transport mechanism.

(50) Bard, A. J.; Faulkner, L. R. *Electrochemical Methods*, 2nd ed.; John Wiley & Sons: New York, 2001.

Table 4. Summary of Crystal Data and Refinement Results for [BMPip][PO_2F_2]

formula	$C_{10}H_{22}F_2NO_2P$
fw	257.26
cryst syst	monoclinic
space group	$P2_1/c$
a/Å	9.7810(4)
b/Å	17.1110(5)
c/Å	15.6039(7)
b/deg	92.977(4)
V/Å^3	2607.99(18)
Z	8
ρ_{calcd}/g cm^{-3}	1.310
T/°C	−173
μ/mm^{-1}	0.223
λ/Å	0.71073
$R_1(F_o^2)^a$	0.0427
$wR_2(F_o^2)^b$	0.1302

$^a R_1 = \sum ||F_o| - |F_c|| / \sum |F_o|$ for $I > 2\sigma(I)$. $^b wR_2 = \{\sum [w(F_o^2 - F_c^2)^2] / \sum [w(F_o^2)^2]\}^{1/2}$ for $I > 2\sigma(I)$.

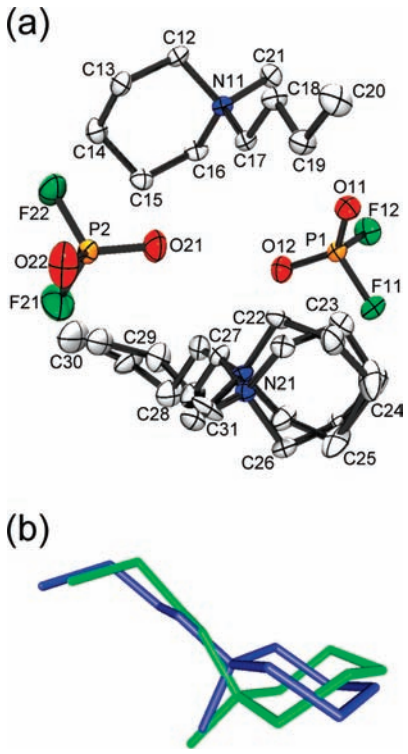

Figure 11. (a) X-ray crystal structure of [BMPip][PO_2F_2]. Thermal ellipsoids are shown at the 50% probability level. (b) View of the disordered $BMPip^+$ cation in [BMPip][PO_2F_2]. Hydrogen atoms are omitted for clarity.

Crystal Structure of [BMPip][PO_2F_2]. The crystal structure of [BMPip][PO_2F_2] was determined using single-crystal X-ray diffraction. Crystal data and refinement results are given in Table 4. The asymmetric unit

(51) Waligoraa, L.; Lewandowski, A.; Gritzner, G. *Electrochim. Acta* **2009**, *54*, 1414–1419.

(52) Zhang, D.; Okajima, T.; Matsumoto, F.; Ohsaka, T. *J. Electrochem. Soc.* **2004**, *151*, D31–D37.

contains two cations and anions (Figure 11a). One of the two cations is disordered into two positions in which the piperidinium rings in chair configurations cross each other (Figure 11b). The *n*-butyl chains intertwine with each other in almost gauche configurations (N21A−C27A−C28A−C29A = 166.6(4)°, C27A−C28A−C29A−C30A = −78.8(6)°, N21B−C27B−C28B−C29B = 176.9(11)°, and C27B−C28B−C29B−C30B = −69.9(16)°, where A and B represent the two groups in the disordered structure). The other cation geometry can be determined well by adopting an ideal chair configuration for the piperidinium ring and anti configurations for the *n*-butyl chain (N11−C17−C18−C19 = 176.3(2)° and C17−C18−C19−C20 = −179.1(2)°). The two $PO_2F_2^-$ anions are fully ordered in C_{2v} symmetry, which satisfies the VSEPR theory. The P−O double bonds (1.450(2)−1.4647(18) Å) are shorter than the P−F single bonds (1.5474(18)−1.5637(15) Å), and the three bond angles in $PO_2F_2^-$ have an order of F−P−F (96.60(9) and 96.18(12)°) < O−P−F (107.27(12)−109.20(10)°) < O−P−O (122.72(12) and 123.73(12)°). Quantum mechanical calculations reproduce the bond angles well but slightly overestimate the bond lengths (Figure 2 and Table S2, Supporting Information). The absence of acidic protons on the cation prevents strong local interactions between the fluorine or oxygen atoms and the hydrogen atom, unlike those for the imidazolium salts,[53] whereas the oxygen atom still has several short contacts to hydrogen atoms (2.3−2.6 Å) compared to the fluorine atoms. This observation agrees with the stronger donor ability of the oxygen atom over that of the fluorine atom in $PO_2F_2^-$ ionic liquids, as shown by the solvatochromic method. Although the X-ray data were collected at 30 °C to determine the structure of the phase above the solid−solid transition temperature (22 °C), the quality of the data was too low to solve the structure. However, this measurement confirmed that the [BMPip][PO_2F_2] phase is not plastic-crystalline but crystalline.

Conclusions

New ionic liquids based on the $PO_2F_2^-$ anion were prepared, and their physical, spectroscopic, electrochemical, and structural properties were characterized. The melting points of the two imidazolium-based salts, [EMIm][PO_2F_2] and [BMIm][PO_2F_2], are below room temperature. The two nonaromatic cation-based salts, [BMPyr][PO_2F_2] and [BMPip][PO_2F_2], are solid at room temperature and exhibit a solid−solid phase transition. The $PO_2F_2^-$ anions in these salts were identified by Raman and IR spectroscopy, and their vibrational frequencies were assigned for the first time on the basis of the results of quantum mechanical calculations. The temperature dependence of conductivity and that of viscosity for the present $PO_2F_2^-$-based ionic liquids were fitted using the VTF equation as for other ionic liquids. The conductivity of [EMIm][PO_2F_2] is comparable to that of the popular ionic liquid electrolyte [EMIm][BF_4] and is higher than that of another popular electrolyte, [EMIm][$N(SO_2CF_3)_2$], with a sufficiently wide electrochemical window, indicating that this ionic liquid is a potential candidate for use as an electrolyte in electrochemical applications. The improvement of stability against hydrolysis by changing the anion from PF_6^- to $PO_2F_2^-$ implies the replacement of popular PF_6^--based ionic liquids with $PO_2F_2^-$-based ionic liquids in synthetic applications especially at elevated temperatures. The strong donor ability of the $PO_2F_2^-$-based ionic liquids facilitates the dissolution of chemical species or electrolytes, which provides significant benefits for certain applications.

Experimental Section

Apparatus and Materials. Volatile materials were handled in a vacuum line constructed of SUS316 stainless steel and PFA. Nonvolatile materials were handled under a dry Ar atmosphere in a glovebox. Acetone (Wako Chemicals, purity >99.5%) was used as purchased. The N-heterocyclic ammonium chlorides ([EMIm][Cl], [BMIm][Cl], [BMPyr][Cl], and [BMPip][Cl]) were prepared by reactions of the amine (1-methylimidazole, Aldrich Chemicals, purity >99%; 1-methylpyrrolidine, Aldrich, purity 97%; and 1-methylpiperidine, Wako Chemicals, purity >99%) with the corresponding chloroalkane (chloroethane, Wako Chemicals, purity >99% or chlorobutane, Wako Chemicals, purity >98%). All of the chlorides were purified by recrystallization from acetonitrile after the addition of ethylacetate. The two potassium salts, [K][PO_3] (Wako Chemicals) and [K][PF_6] (Aldrich purity >99.5%), were dried under a vacuum at 100 °C for a few days before use. Ferrocene was used as purchased (Aldrich, purity 98%). The ionic liquids used for comparison ([EMIm][BF_4], [BMIm][BF_4], [BMIm][PF_6], and [BMIm][$N(SO_2CF_3)_2$]) were either purchased (Kanto Kagaku) or prepared according to the literature method ([EMIm][$N(SO_2CF_3)_2$])[6] and dried prior to use. Typical synthetic procedures for the $PO_2F_2^-$ salts are described below.

Synthesis of [K][PO_2F_2]. Two synthetic routes for [K][PO_2F_2] have been reported. One is the reaction of $[K]_2[HPO_4]$, $[NH_4][HF_2]$, and $OC(NH_2)_2$, and the other is the reaction of [K][PO_3] and [K][PF_6].[18,54] Although both routes yield products with sufficient purity for the present study, the former (reaction in molten urea) is not suitable as a gram-scale laboratory synthesis. The following is a typical procedure using the latter reaction. The two salts, [K][PO_3] (12.974 g, 0.10988 mol) and [K][PF_6] (10.113 g, 0.05494 mol), were loaded into a Pt crucible under a dry Ar atmosphere. The Pt crucible was placed in a Monel airtight vessel. The Monel vessel was sealed using a Teflon O-ring and a stainless lid with a stainless valve. After the removal of moisture under a vacuum at 100 °C overnight, the vessel was heated to 320 °C and kept at this temperature for three days. The stainless lid was cooled by water circulation during the reaction to avoid damage to the Teflon O-ring. After the reaction finished, the vessel was cooled to room temperature and evacuated for 1 h to remove any volatiles. The purity of the obtained sample was confirmed by Raman spectroscopy and X-ray powder diffraction.

Synthesis of [EMIm][PO_2F_2]. Equimolar amounts of [EMIm][Cl] (3.000 g, 20.46 mmol) and [K][PO_2F_2] (2.869 g, 20.48 mmol) were loaded into a polypropylene vessel with acetone (10 mL) as a solvent. The mixture was stirred for three days, and the resulting white precipitate of KCl was removed by filtration. The crude acetone solution of [EMIm][PO_2F_2] was purified by column chromatography through an activated alumina (Wako Chemicals, 75 μm) column. The solvent was initially removed under a vacuum at room temperature and then later at 70 °C to yield [EMIm][PO_2F_2] as a colorless liquid (2.590 g, 12.21 mmol). Testing for the presence of residual chloride impurities with a silver nitrate solution gave no

(53) Matsumoto, K.; Hagiwara, R. *J. Fluorine Chem.* **2007**, *128*, 317–331.

(54) Schülke, U.; Kayser, R. *Z. Anorg. Allg. Chem.* **1991**, *600*, 221–226.

precipitation of silver chloride. Anal. Calcd for $C_6H_{11}N_2O_2F_2P_1$: C, 33.97; H, 5.23; N, 13.21; F, 17.91. Found: C, 33.72; H, 5.21; N, 13.23; F, 17.67.

Synthesis of [BMIm][PO_2F_2]. The same procedure as that for [EMIm][PO_2F_2] was used. Reaction of [BMIm]Cl (10.000 g, 57.322 mmol) and K[PO_2F_2] (8.029 g, 57.321 mmol) gave [BMIm][PO_2F_2] as a colorless liquid (9.010 g, 37.511 mmol). Anal. Calcd for $C_8H_{15}N_2O_2F_2P_1$: C, 40.01; H, 6.29; N, 11.66; F, 15.82. Found: C, 40.31; H, 6.12; N, 11.66; F, 15.54.

Synthesis of [BMPyr][PO_2F_2]. The same procedure as that for [EMIm][PO_2F_2] was used. Reaction of [BMPyr]Cl (3.500 g, 19.72 mmol) and K[PO_2F_2] (2.763 g, 19.73 mmol) gave [BMPyr][PO_2F_2] as a colorless solid (3.510 g, 14.45 mmol). Anal. Calcd for $C_9H_{20}N_1O_2F_2P_1$: C, 44.44; H, 8.29; N, 5.76; F, 15.62. Found: C, 43.74; H, 8.24; N, 5.56; F, 14.92.

Synthesis of [BMPip][PO_2F_2]. The same procedure as that for [EMIm][PO_2F_2] was used. Reaction of [BMPip]Cl (10.000 g, 52.123 mmol) and K[PO_2F_2] (7.305 g, 52.15 mmol) gave [BMPip] [PO_2F_2] as a colorless solid (8.100 g, 31.49 mmol). Anal. Calcd for $C_{10}H_{22}N_1O_2F_2P_1$: C, 46.69; H, 8.62; N, 5.44; F, 14.77. Found: C, 46.34; H, 8.72; N, 5.39; F, 14.50.

Spectroscopic and Thermal Analyses. Raman spectra were recorded (FTS-175C, Bio-Rad Laboratories) at room temperature using the 1064 nm line of a Nd:YAG laser as the excitation line. The samples for Raman spectroscopy were loaded in Pyrex glass tubes (5 mm o.d.) under dry Ar and sealed with a plastic cap. Infrared spectra were recorded (FTS-165, BIO-RAD Laboratories) at room temperature. The samples for IR spectroscopy were sandwiched between a pair of AgCl windows fixed in a stainless airtight cell under dry Ar. Nuclear magnetic resonance spectra of ^{31}P (121.5 MHz) were recorded on a Varian Mercury-300 spectrometer at 25 °C. Deuterated acetonitrile was used as a solvent. Phosphoric acid in deuterated acetonitrile was used as an external standard. Differential scanning calorimetry (DSC-60, Shimadzu) was performed under a dry Ar gas flow or in the air. The samples for DSC measurement were loaded into an aluminum airtight cell under dry Ar. A scan rate of 5 °C min^{-1} was used. Thermogravimetry (DTG-60H, Shimadzu) was performed under a dry Ar gas flow or normal air conditions. Samples for TG measurement were loaded in an aluminum cell under dry Ar. A scan rate of 5 °C min^{-1} was used.

Measurement of Physical and Electrochemical Properties. Water content was measured using a Karl Fischer moisture analyzer (MKC-510N, Kyoto Electronics Mfg. Co.). Liquid samples were directly introduced into the analyzer. Solid samples were dissolved into ethanol (Wako Chemicals, water content 27 ppm) and introduced into the analyzer as ethanol solutions. Conductivity was measured by the AC impedance technique using a cell with platinum disk electrodes calibrated using KCl standard aqueous solution. Viscosity was measured with a cone−plate rheometer (DV-II+Pro, Brookfield Engineering Laboratories, Inc.). Density was measured by weighing the sample in a calibrated PFA vessel. Electrochemical measurements were performed using a Pt or glassy carbon working electrode and a Pt counter electrode with an electrochemical measurement system (HZ-3000, Hokuto Denko). The reference electrode was made of silver wire immersed in $EMImBF_4$ containing 0.05 M $AgBF_4$ that was separated from the electrolyte by porous Vycor glass.

X-Ray Diffraction Analyses. a. Powder Diffraction. The sample was transferred into a quartz capillary (0.5 mm o.d., previously dried under a vacuum at 500 °C) under a dry Ar atmosphere. The capillary was tentatively plugged with vacuum grease and sealed using an oxygen burner. The sample was centered on an X-ray diffractometer (R-axis Rapid II, Rigaku) equipped with an imaging plate area detector (using the program RAPID XRD 2.3.3[55]) and graphite-monochromated Mo Kα radiation (0.71073 Å). The ϕ angle was rotated at a rate of 1° s^{-1}, and the ω and χ angles were fixed at 20° and 0°, respectively, during the collection (1000 s).

b. Single-Crystal Diffraction. Crystals of [BMPip][PO_2F_2] were grown by slow cooling of molten [BMPip][PO_2F_2] in a polypropylene vessel without a solvent. Suitable crystals were mounted in quartz capillaries under dry Ar and sealed as for the powder sample. The single crystal used for data collection was a colorless transparent block measuring 0.15×0.15×0.15 mm^3 and was centered on the diffractometer (R-axis Rapid II, Rigaku controlled by the program RAPID AUTO 2.40[56]). Data collection was performed at −173 °C and consisted of 12 ω scans (130−190°, 5°/frame) at fixed ϕ (0°) and χ (45°) angles and 32 ω scans (0−160°, 5° per frame) at fixed ϕ (180°) and χ (45°) angles. The exposure time was 1200 s deg^{-1}. Integration, scaling and absorption corrections were performed using RAPID AUTO 2.40. The structure was solved using SIR-92[57] and refined by SHELXL-97[58] linked to Win-GX.[59] Anisotropic displacement factors were introduced for all atoms except for hydrogen.

Calculations. The energy-minimized gas-phase structures and vibrational data were calculated at the HF, B3LYP, PBE1PBE, MPW1PW91, and MP2 levels of theory using cc-pVTZ and aug-cc-pVTZ basis sets. The NBO analyses were performed for the B3LYP, PBE1PBE, and MPW1PW91 optimized local minima.[16] Quantum mechanical calculations were carried out using the program Gaussian 03.[60]

Acknowledgment. This work was financially supported by a Grant-in-Aid for Scientific Research (A) from the Japan Society for the Promotion of Science. The authors would like to thank Professor Seijiro Matsubara and Assistant Professor Takuya Kurahashi of Graduate School of Engineering, Kyoto University for their kind help in NMR measurements.

Supporting Information Available: Calculated geometrical parameters and partial atomic charges, experimental and calculated vibrational frequencies and intensities, VTF equation parameters, electrochemical parameters, X-ray powder diffraction patterns, TG traces, digital images of ionic liquids, visible spectra, NMR spectra, electrochemical diagrams, and additional relevant literature. This material is available free of charge via the Internet at http://pubs.acs.org.

(55) *RAPID XRD*, version 2.3.3; Rigaku Corporation: Tokyo, Japan, 1999.

(56) *RAPID AUTO*, version 2.40; Rigaku Corporation: Tokyo, Japan, 2006.

(57) Altomare, A.; Burla, M. C.; Camalli, M.; Cascarano, G.; Giacovazzo, C.; Gugliardi, A.; Polidori, G. *J. Appl. Crystallogr.* **1994**, *7*, 435.

(58) Sheldrick, G. M. *SHELXL-97*; University of Göttingen: Göttingen, Germany, 1998.

(59) Farrugia, L. J. *J. Appl. Crystallogr.* **1999**, *32*, 837–838.

(60) Frisch, M. J. et al. *Gaussian 98*, revision E.01; Gaussian, Inc.: Pittsburgh, PA, 2003.